Solutions of the Schrödinger-Poisson equations for $n-$dimensional states

I. Álvarez-Rios* and F. S. Guzmán†

Instituto de Física y Matemáticas, Universidad Michoacana de San Nicolás de Hidalgo, Edificio C-3, Cd. Universitaria, 58040 Morelia, Michoacán, México.
*e-mails: *ivan.alvarez@umich.mx; †francisco.s.guzman@umich.mx*

Received 15 March 2024; accepted 5 November 2024

We construct stationary solutions for the Schrödinger-Poisson system of equations for $n-$dimensional states. We find that these have the solitonic profile of the ground state solution of the scalar case $n = 1$ for all the fields. We numerically study the cases $n = 1, 2, 3, 4, 5$, because these multifield scenarios have been proposed as a generalization of the scalar field dark matter $n = 1$, specially state vectors with $n = 3$ and $n = 5$ fields. In order to verify the formation of core-halo density profiles we simulate multi-core mergers of equilibrium configurations and show that every field accommodates itself with its own solitonic+halo profile, showing in this way that equilibrium solutions are attractor cores.

Keywords: Self-gravitating systems; dark matter; Bose condensates.

DOI: https://doi.org/10.31349/RevMexFis.71.020704

1. Introduction

Ultralight Bosonic Dark Matter or Scalar Dark Matter (SDM), currently under study, presents intriguing implications. While it behaves similarly to Cold Dark Matter (CDM) on large scales, at local galactic scales, it exhibits a core-tail structure due to its small mass, typically of order $10^{-24} - 10^{-20}\mathrm{eV}/c^2$. This small mass results in a large de Broglie wavelength, preventing the formation of cuspy density profiles. Consequently, this property is believed to offer a potential solution to the cusp-core and too big to fail problems associated with CDM. Further details and constraints of this dark matter model are extensively discussed in recent reviews [1-5].

Being the core formation surrounded by a halo the signature of this ultralight bosonic multiple or single wave functions, once the SDM has shown to have interesting properties it is possible to formulate other variants of the idea. One of them is the use of multiple scalar fields, for example triplets that constitute spin-1 fields. In Ref. [6] a comparative analysis of the ultralight Scalar Dark Matter (SDM) and Vector Dark Matter (VDM) made of a three-component vector field is developed. Their investigation is based on the analysis of multicore mergers with the aim of finding characteristic differences of each dark matter model. Based on simulations it is found the formation of core-tail structures, and it is observed that interference effects are less pronounced in VDM compared to SDM, potentially yielding discrepancies in the heating of luminous matter. Other aspects are also studied, including the core-halo mass scaling relation and structural differences between SDM and VDM in the envelope region. The analysis was extended for different degrees of correlation between the field components in Ref. [7], where the aim is the formation of Proca stars from structure formation initial conditions.

In the context of structure formation, the core formation of multiple scalar field dark matter core formation can be seen in Refs. [8,9]. Later on in Ref. [10] the condensate formation through kinetic relaxation is studied for $n = 2s + 1$ components, in particular spin$-s$ fields with $s = 1, 2$, whose relaxation times are modeled for equal and unequal boson masses between the components of the field.

In this paper we concentrate in the core-tail formation simulations using multi-core mergers like in Ref. [6]. Unlike in Refs. [6,7] where VDM is studied, we study the case with $n = 1, 2, 3, 4, 5$, that includes the cases $s = 1, 2$ in Ref. [10] and the intermediate multifield non-spin fields $n = 2, 4$. We start from the construction of stationary solutions and study their stability along with their attractor properties. We find that the core is formed in all cases, not only as a whole but each component accommodates in a core that can be fitted with the well known solitonic profile of the ground state stationary solution of the Schrödinger-Poisson system of equations [11,12].

The paper is organized as follows. In Sec. 2 we write down the equations describing the evolution of the system and in Sec. 3 we construct stationary solutions. In Sec. 4 we test the stability of solutions whereas in Sec. 5 we show their attractor properties. Finally in Sec. 6 we draw some conclusions.

2. Model and equations

The SP equations for an $n - d$ dimensional state, with $\hbar$ and the boson mass m_B absorbed constants reads

$$i\partial_t \vec{\Psi} = -\frac{1}{2}\nabla^2 \vec{\Psi} + V\vec{\Psi}, \tag{1}$$

$$\nabla^2 V = \rho - \langle\rho\rangle, \tag{2}$$

where $\vec{\Psi} = (\Psi_1, \Psi_2, ..., \Psi_n)$, V is the gravitational potential generated by the total density $\rho = \sum_{j=1}^{n} |\Psi_j|^2$, and $\langle\rho\rangle$ represents the average of the total density over the entire domain.

An important point to emphasize is that the system (1)-(2) remains invariant under the λ-transformation:

$$\{\vec{x}, \vec{\Psi}, V, \rho\} \rightarrow \{\lambda^{-1}\vec{x}, \lambda^2\vec{\Psi}, \lambda^2 V, \lambda^4\rho\}, \tag{3}$$

just like in the scalar case $n = 1$ [12].

3. Stationary solution

To find stationary solutions of the system (1)-(2), we assume that each component of the state vector behaves like a stationary wave: $\Psi_j = \psi_j e^{-i\omega_j t}$, where ψ_j are real functions with $j = 1, 2, ..., n$. Furthermore, we assume that the system has spherical symmetry. Under these assumptions, the system (1)-(2) can be expressed as a first-order system with respect to the radial coordinate r:

$$\frac{d\psi_j}{dr} = \frac{\phi_j}{r^2}, \tag{4}$$

$$\frac{d\phi_j}{dr} = 2\left(V - \omega_j\right)\psi_j r^2, \tag{5}$$

$$\frac{dM}{dr} = r^2\rho, \tag{6}$$

$$\frac{dV}{dr} = \frac{M}{r^2}. \tag{7}$$

To determine solutions of these equations, boundary conditions must be specified: $\psi_j(0) = \psi_j^c$, $\phi_j = 0$, $M(0) = 0$, $V(0) = V_c$, and $\lim_{r\to\infty}\psi_j = \lim_{r\to\infty}\phi_j = 0$. It is worth noting that the choice of V_c can be arbitrary because the system is invariant under the transformation $V \rightarrow V + V_0$, where $\omega_j \rightarrow \omega_j + V_0$ for some constant V_0.

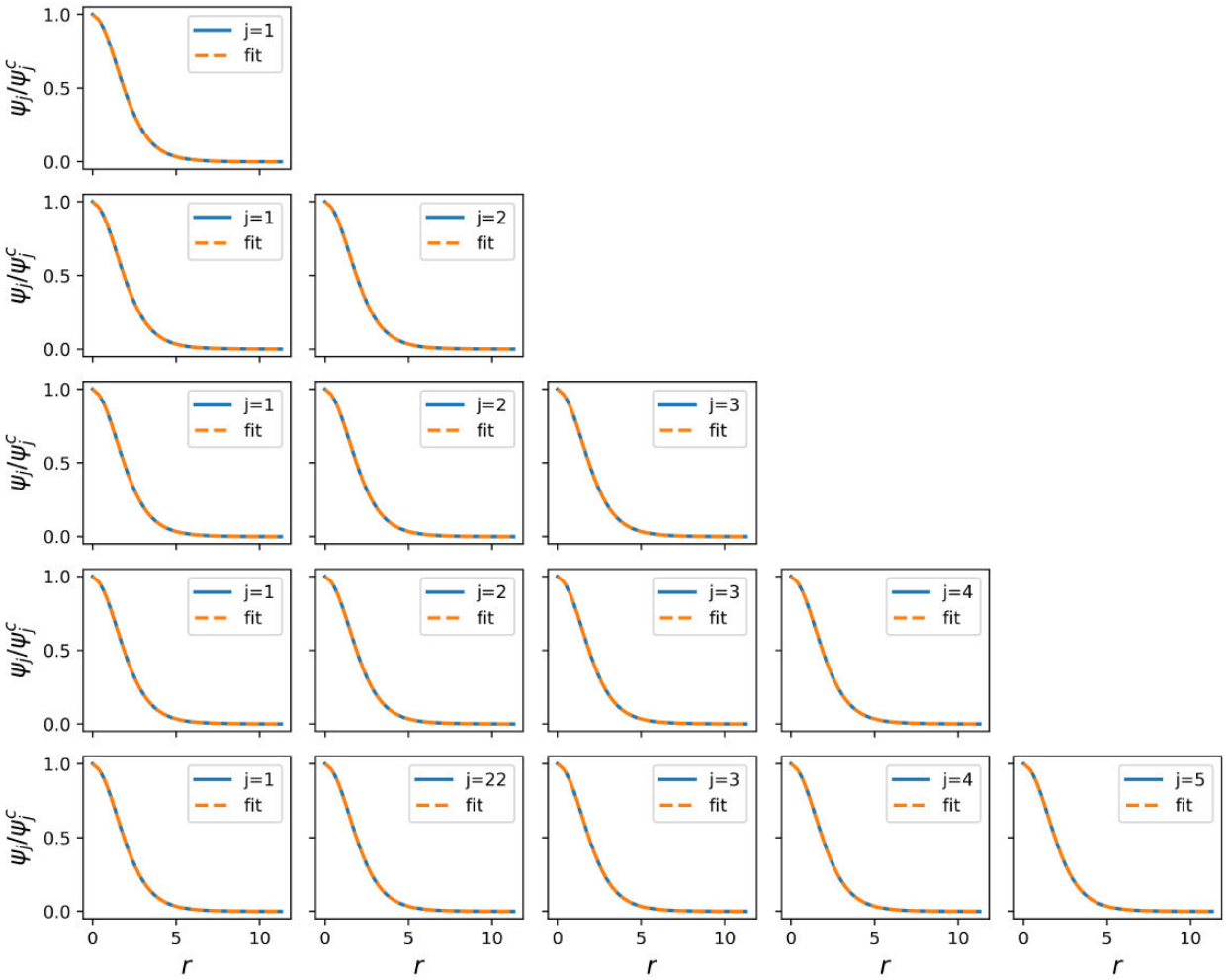

FIGURE 1. Each row displays the numerical solutions for the eigenproblem (4-7) of each component of the state vector, along with the corresponding fitted wave field according to formula (13). The first, second, third, fourth and fifth rows correspond to the solutions with $n = 1$, 2, 3, 4 and 5, respectively. The amplitude of the different states is restricted to the condition $\rho_c = 1$.

Notice that if we redefine the variables through the relations $\psi_j = \psi_j^c\tilde{\psi}_j$ and $\phi_j = \psi_j^c\tilde{\phi}_j$, the new variables satisfy the boundary conditions $\tilde{\psi}_j(0) = 1$, $\tilde{\phi}_j(0) = 0$, and $\lim_{r\to\infty}\tilde{\psi}_j = \lim_{r\to\infty}\tilde{\phi}_j = 0$. We also assume that all components of the state vector have the same energy, *i.e.*, $\omega_j = \omega$. This is a necessary condition when the mass of the various components is the same. Consequently, the first two Eqs. (4-5) become independent of the j index, as they represent the same equations with identical boundary conditions. This reduction leads the system to the following equations:

$$\frac{d\tilde{\psi}}{dr} = \frac{\tilde{\phi}}{r^2}, \tag{8}$$

$$\frac{d\tilde{\phi}}{dr} = 2\left(V-\omega\right)\tilde{\psi}r^2, \tag{9}$$

$$\frac{dM}{dr} = r^2\rho_c\tilde{\psi}^2, \tag{10}$$

$$\frac{dV}{dr} = \frac{M}{r^2}, \tag{11}$$

where $\rho_c = ||\vec{\psi_c}||^2 = \sum_{j=1}^{n}(\psi_j^c)^2$. Now, let us recall that in the case of a single field, the solution can be uniquely determined by the condition $\psi(0) = 1$ or, equivalently, $|\psi(0)|^2 = 1$. This can be generalized to the n-dimensional case by setting the value $\rho_c = 1$ according to the invariance (3), where we now have $n-1$ degrees of freedom to choose the values ψ_j^c over $S^{n-1} = \{\vec{\psi_c} \in \mathbb{R}^n \,|\, \rho_c = 1\}$. Note that the system of dimension n is equivalent to the system with $n = 1$, but each component of the n-dimensional state vector is rescaled by the amplitude ψ_j^c related to the stationary solution of the system with $n = 1$.

Considering this, it is known that the density associated with the ground state can be approximated by the formula [13]:

$$\rho(r) = \rho_c\left[1 + 0.091\left(\frac{r}{r_c}\right)^2\right]^{-8}. \tag{12}$$

In this formula $\rho_c \approx (1.3056/r_c)^4$ is the central density, and r_c is the core radius. The components of the state vector in the $n-$dimensional case can be expressed as:

$$\psi_j(r) = \psi_j^c\left[1 + 0.091\left(\frac{r}{r_c}\right)^2\right]^{-4}, \tag{13}$$

where the amplitudes ψ_j^c must satisfy the relation $\sum_{j=1}^{n}|\psi_j^c|^2 = (1.3056/r_c)^4$ for an arbitrary value of r_c. The mass associated with each component of the state vector is given by the expression:

$$M_j = 4\pi\int_0^\infty |\psi_j(r)|^2 r^2 dr \approx 11.587|\psi_j^c|^2 r_c^3. \tag{14}$$

Then, the total mass of the density distribution satisfies $M = \sum_{j=1}^{n} M_j \approx 33.667/r_c$.

The assumption that all components have the same eigenvalue can be justified through the numerical solution of the original system for specific amplitudes in each component, as illustrated in Fig. 1. Moreover, in the context of bosonic dark matter, if the bosons are all of the same mass, there is no other option that accomodate in varios states with the same eigenvalue. The figure presents the solutions of the original system alongside the fitting provided by Eq. (13) for state vector with dimension $n = 1$, 2, 3, 4 and 5. With these results, we demonstrate that the fitting formula can be employed to approximate the ground states of the n-dimensional case. However, it is essential to investigate the impact when using this approximation, such as the initial conditions for the time-dependent system.

4. Stability of solutions

In a general context, the assessment of stability for approximated ground states with profile (13) involves the solution of system (1)-(2). We inject the configurations in a three-dimensional domain described with Cartesian coordinates $D = [x_{\min}, x_{\max}]^3$, employing an extension of CAFE [14,15]. The CAFE code uses an implicit Crank-Nicholson scheme using the Fast Fourier Transform (FFT) to evolve the state vector, and at each step of evolution, the Poisson equation is solved also using a FFT method.

For the stability analysis, a trivial perturbation occurs, where the ground state is disturbed by its approximation and the truncation error in the numerical methods during evolution. Each component of the state vector experiences an identical disturbance.

To assess the stability of the fundamental state of the n-dimensional system, we choose initial conditions based on the approximations of Eq. (13). In other words, the initial conditions for the system (1)-(2) for each component of the state vector are

$$\Psi_j(\vec{x}, 0) = \psi_j(|\vec{x}|), \qquad j = 1, 2, ..., n, \tag{15}$$

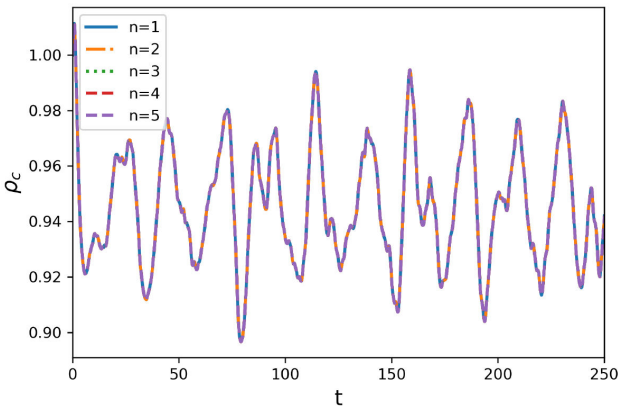

FIGURE 2. Central value of density as a function of time for state vectors of dimension $n = 1$, 2, 3, 4 and 5, demonstrating that the oscillation of the ground state is independent of the dimension of the system.

where $\vec{x} \in D$ are the Cartesian coordinates. In this case, the system can be reduced to the $n = 1$ problem, introducing a new variable as in the stationary case: $\bar{\Psi}_j = \Psi_j/\psi_j^c$, which is independent of the index j. The system takes on the form:

$$i\partial_t \bar{\Psi} = -\frac{1}{2}\nabla^2 \bar{\Psi} + V\bar{\Psi}, \tag{16}$$

$$\nabla^2 V = \rho_c(|\bar{\Psi}|^2 - \langle|\bar{\Psi}|^2\rangle), \tag{17}$$

with the initial condition

$$\bar{\Psi}(\vec{x}, 0) = \left[1 + 0.091\left(\frac{|\vec{x}|}{r_c}\right)^2\right]^{-4}. \tag{18}$$

Assuming normalized states ($\rho_c = 1$), the system reduces exactly to the scalar problem ($n = 1$), affirming the stability of the fundamental states, as indicated in Ref. [12]. Additionally, a stability test of the complete system is conducted by evolving the n-dimensional case for $n = 1$, 2, 3, 4 and 5. A point is chosen randomly for $\vec{\psi}_c \in S^{n-1}$, where each component of the state vector $\vec{\psi}_c$ is non-zero. The system is evolved in the domain $D = [-10, 10]^3$, which is over seven times larger than the size of the core radius r_c, ensuring that boundary conditions have a negligible impact on the evolution of the ground state when $n = 1$ [15], for a duration of 250 time units.

The central value of the density is monitored, as shown in Fig. 2. The figure illustrates how the density oscillates near its initial value, indicating stability against trivial perturbations independently of the dimension of the system.

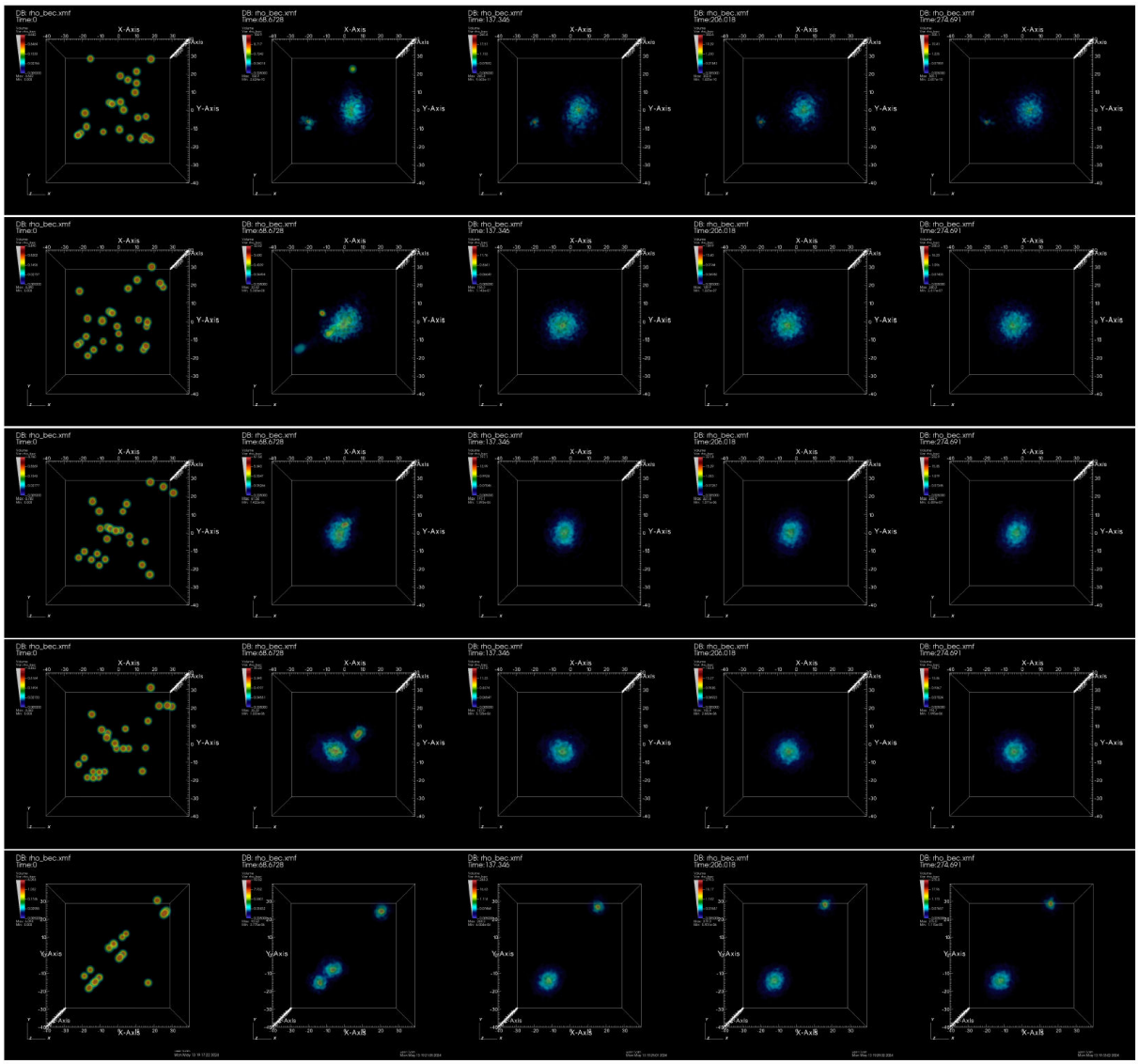

FIGURE 3. Dynamics of the density profile illustrated with five snapshots at times $t = 0$, 69, 137, 206, and 275 in each column. First, second, third, fourth and fifth rows correspond to state vector of dimension $n = 1$, 2, 3, 4 and 5, respectively. In the case of $n = 5$ notice the formation of two cores, which is casual due to the randomness of initial conditions; the fittings of density for this case are performed over the bigger one.

5. Attractor properties

In order to investigate whether the density of the fundamental state is an attractor in the n-dimensional system, we carry out simulations for $n = 1$, 2, 3, 4 and 5. As initial conditions for the system, we place $24/n$ solitons of each state for the cases $n = 1$, 2, 3 and 4, whereas for $n = 5$ we place 5 solitons in each state. These components of the state vector are randomly distributed over the domain $D = [-40, 40]^3$ and random radii with $\lambda \in [1.25, 1.5]$ of the scaling relations (3). The domain is discretized with a spatial resolution $h = 5/8$ and a time resolution that satisfies the Courant condition $\Delta t/h^2 < 0.25$. The system is evolved during 275 units of code time, which corresponds to 14Gyr for a boson mass of 10^{-22} eV.

Figure 3 shows snapshots of the density profile at times $t \sim 0, 69, 137, 206$, and 275 in each column, for state vector of dimension $n = 1, 2, 3, 4$ and 5 in each row. Regardless of the dimension n, a core-halo structure forms over time, as mentioned in more detail in Ref. [15] for $n = 1$. We calculate

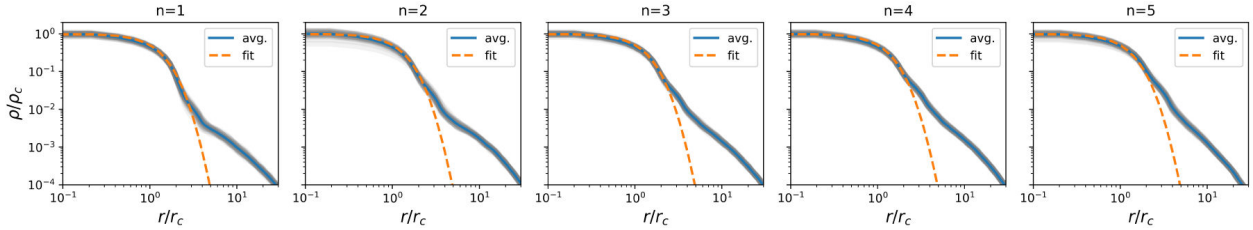

FIGURE 4. The temporal and spatial average of the density profile is depicted as a function of the radial coordinate r, represented by the solid blue line. Additionally, a fit according to Eq. (12) is illustrated using the dotted line for state vectors of dimensions $n = 1$, 2, 3, 4 and 5 in each column. Finally, the grey thick line on top of the average is the latest 30 snapshots used to calculate the average of density once the structure has relaxed.

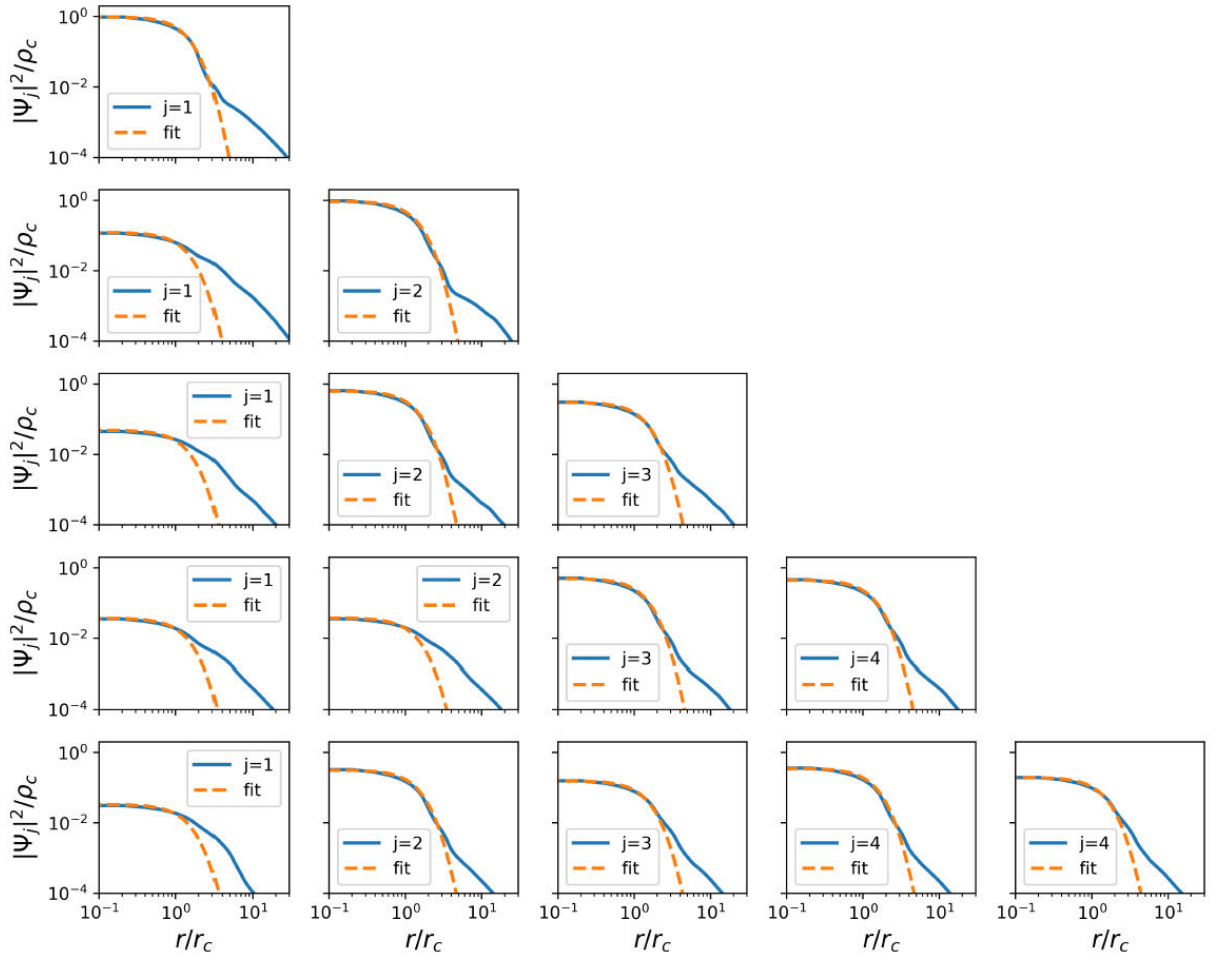

FIGURE 5. Each row displays the temporal and spatial normalized averages of individual components of the state vector with dimensions $n = 1$, 2, 3, 4 and 5, respectively, represented by solid lines. Dotted lines correspond to core fittings with the square of Eq. (13).

TABLE I. Parameters obtained from fits for r_c and $|\psi_j^c|^2$ for the multimerger simulation for a state vector of dimension n =1, 2, 3, 4 and 5.

n	r_c	$\|\psi_1^c\|^2$	$\|\psi_2^c\|^2$	$\|\psi_3^c\|^2$	$\|\psi_4^c\|^2$	$\|\psi_5^c\|^2$
1	0.3264 ± 0.0020	$(1.3056/r_c)^4$				
2	0.3630 ± 0.0025	20.96 ± 1.034	159.8 ± 4.372			
3	0.3484 ± 0.0022	9.806 ± 0.5849	127.9 ± 3.154	60.91 ± 1.415		
4	0.3583 ± 0.0023	6.547 ± 0.2835	6.672 ± 0.3336	88.25 ± 2.245	80.07 ± 1.975	
5	0.3390 ± 0.0020	7.405 ± 0.3719	70.55 ± 1.846	34.96 ± 0.7766	78.61 ± 2.079	43.42 ± 0.9572

a spatial average over the solid angle and time in the last 100 units of time. This average has the solitonic core surrounded by the halo profile (12) can be fitted to this average by tuning the parameter r_c, and the results are illustrated in Fig. 4 Once the configuration relaxes, it oscillates both in time and in space around this average profile. In this figure we plot the latest 30 snapshots of the evolution that produces a thick grey line around the average density.

Taking a step further, the analysis extends to each component of the state vector. By fixing the value of r_c obtained from adjusting the average density, we determine the appropriate amplitudes of the squared modules of each component according to Eq. (13). The results, depicted in Fig. 5, reveal that each component exhibits a core with a solitonic profile, consistent with the ground state of the n-dimensional system. The figures are normalized with respect to the values r_c and $\rho_c = (1.3056/r_c)^4$, which can be found in Table I along with the parameters for each component of the state vector. Two observations are in turn: the first one is that these are averaged density profiles, as dynamic and space-dependent, just likewise those structures found in structure formation simulations, something not everywhere pointed out and that needs to be taken with care; the second one is that the averaged density profile of each component corresponds to those of the solutions constructed in Sec. 3, showing in this way that the assumption of equal mass of each component leads to equal eigenfrequencies of the solution, which can be seen as an independent proof of concept of the equal eigen-frequency assumption, because here we do not consider stationarity, not even spherical symmetry, we show that simply these configurations form in an attractor way.

6. Conclusions

We have described the equivalence between the ground state of the n-dimensional system and the scalar case ($n = 1$), supporting the hypothesis that they share the same eigenenergy by directly solving the stationary problem. The dynamics of the approximation of the n-dimensional ground state are analyzed by directly evolving the vectorial SP system. We find that the ground state is stable independently of n for n =1, 2, 3, 4, 5, and this stability can be reduced to the case of the scalar problem with $n = 1$. Finally, we conducted simulations of multi-core mergers with initial conditions with zero angular momentum and confirmed that the ground state remains an attractor of the system for the values of n explored.

Acknowledgments

Iván Álvarez receives support within the CONACyT graduate scholarship program under the CVU 967478. This research is supported by grants CIC-UMSNH-4.9 and CONACyT Ciencias de Frontera Grant No. Sinergias/304001. The runs were carried out in the facilities of the Laboratorio Nacional de Cómputo de Alto Desempeño under grant No. 1-2024.

1. A. Suárez, V. H. Robles, and T. Matos, A Review on the Scalar Field/Bose-Einstein Condensate Dark Matter Model, *Astrophys. Space Sci. Proc.* **38** (2014) 107, https://doi.org/10.1007/978-3-319-02063-19.
2. L. Hui, Wave dark matter, *Annual Review of Astronomy and Astrophysics* **59** (2021) 247, https://doi.org/10.1146/annurev-astro-120920-010024.
3. E. G. M. Ferreira, Ultra-Light Dark Matter, *The Astronomy and Astrophysics Review* **29** (2021) 7, https://doi.org/10.1007/s00159-021-00135-6.
4. P.-H. Chavanis, Self-gravitating bose-einstein condensates, in Quantum Aspects of Black Holes, edited by Xavier Calmet (Springer International Publishing, Cham, 2015) pp. 151, https://doi.org/10.1007/978-3-319-10852-06.
5. J. C. Niemeyer, Small-scale structure of fuzzy and axion-like dark matter, *Progress in Particle and Nuclear Physics* **113** (2020) 103787, https://doi.org/10.1016/j.ppnp.2020.103787.
6. M. A. Amin, Mudit Jain, Rohith Karur, and Philip Mocz, Small-scale structure in vector dark matter, *Journal of Cosmology and Astroparticle Physics* **2022** (2022) 014, https://doi.org/10.1088/1475-7516/2022/08/014.
7. J. Chen, X. Du, M. Zhou, A. Benson, and D. J. E. Marsh, Gravitational boseeinstein condensation of vector/hidden pho-

ton dark matter, *Phys. Rev. D* **108** (2023) 083021, https://doi.org/10.1103/PhysRevD.108.083021.

8. H. Huang, H.-Y. Schive, and T. Chiueh, Cosmological simulations of twocomponent wave dark matter, *Monthly Notices of the Royal Astronomical Society* **522** (2023) 515, https://doi.org/10.1093/mnras/stad998.
9. N. Glennon, N. Musoke, and C. Prescod- Weinstein, Simulations of multi eld ultralight axionlike dark matter, *Phys. Rev. D* **107** (2023) 063520, https://doi.org/10.1103/PhysRevD.107.063520.
10. M. Jain, M. A. Amin, J. Thomas, and Wisha Wanichwecharungruang, Kinetic relaxation and bose-star formation in multicomponent dark matter, *Phys. Rev. D* **108** (2023) 043535, https://doi.org/10.1103/PhysRevD.108.043535.
11. F. S. Guzmán and L. Arturo Ure na López, Evolution of the Schrödinger-Newton system for a self-gravitating scalar field, *Phys. Rev. D* **69** (2004) 124033, https://doi.org/10.1103/PhysRevD.69.124033.
12. F. S. Guzmán and L. Arturo Ure na López, Gravitational cooling of self-gravitating bose condensates, *The Astrophysical Journal* **645** (2006) 814, https://doi.org/10.1086/504508.
13. H.-Y. Schive, T. Chiueh, and T. Broadhurst, Cosmic Structure as the Quantum Interference of a Coherent Dark Wave, *Nature Phys*. **10** (2014) 496, https://doi.org/10.1038/nphys2996.
14. I. Álvarez-Rios and F. S Guzmán, Exploration of simple scenarios involving fuzzy dark matter cores and gas at local scales, *Monthly Notices of the Royal Astronomical Society* **518** (2022) 3838, https://doi.org/10.1093/mnras/stac3395.
15. I. Álvarez-Rios, F. S. Guzmán, and Paul R. Shapiro, Effect of boundary conditions on structure formation in fuzzy dark matter, *Phys. Rev. D* **107** (2023) 123524, https://doi.org/10.1103/PhysRevD.107.123524.